Vol 17 No 4, April 2008
1674-1056/2008/17(04)/1312-06

Chinese Physics B

© 2008 Chin. Phys. Soc.
and IOP Publishing Ltd

Simulation study on reconstruction model of three-dimensional temperature distribution within visible range in furnace*

Liu Dong(刘 冬), Wang Fei(王 飞)†, Huang Qun-Xing(黄群星),
Yan Jian-Hua(严建华), Chi Yong(池 涌), and Cen Ke-Fa(岑可法)

State Key Laboratory of Clean Energy Utilization, Zhejiang University, Hangzhou 310027, *China*

(Received 7 May 2007; revised manuscript received 12 October 2007)

This paper presents a reconstruction model of three-dimensional temperature distribution in furnace based on radiative energy images captured by charge-coupled device (CCD) cameras within the visible wavelength range. Numerical simulation case was used in this study and a zigzag eccentric temperature distribution was assumed to verify the model. Least square QR-factorization (LSQR) method was introduced to deal with reconstruction equation. It is found that the reconstructed temperature distributions in low-temperature areas had some fluctuations and high-temperature areas were reconstructed well. The whole reconstruction relative error was mainly due to errors in low-temperature areas and the relative error for highest-temperature reconstruction was quite small.

Keywords: three-dimensional temperature distribution, radiative energy images, visible range, charge-coupled device

PACC: 4440, 0720D, 8690

1. Introduction

Temperature measurement in furnace plays an important role in combustion researches. Variation of temperature directly reflects the change of combustion condition in furnace. In recent years many studies have been conducted for the reconstruction of temperature distribution in the target space by using some kinds of inverse problem of radiation. Li *et al*[1−3] and Liu *et al*[4,5] have reconstructed the temperature distributions in the plane-parallel, spherical, cylindrical, semitransparent, and grey media by the inverse analysis of the data of the radiation intensities exiting the boundaries. Silvaneto *et al*[6] presented an inverse radiation analysis for simultaneous estimation of optical thickness, single scattering albedo and the coefficients of phase function for an anisotropic scattering plane-parallel medium. And much attention has been focused on temperature distribution reconstruction from radiative energy images captured by charge-coupled device (CCD) cameras. Liu *et al*[7] used truncated singular value decomposition (TSVD) to reconstruct three-dimensional (3D) flame temperature distribution in furnace and analysed the ill-posed characteristics of reconstruction problem. Zhou *et al*[8,9] have reconstructed the temperature distribution in the two-dimensional (2D) area without considering the scattering, and improved a modified Tikhonov regularization method for solving the inverse problem of 3D temperature distribution; but their studies were based on ideal CCD cameras which could receive radiative energy within the whole thermal radiative wavelength range. Monte Carlo simulation has been widely used in many areas, such as the works of Guan *et al*,[10] Farmer *et al*[11] and Wang *et al*.[12] In this paper Monte Carlo method is used for simulating radiative energy propagation.

As mentioned above, formulas for 3D temperature distribution reconstruction in available studies were made for the whole wavelength range instead of visible wavelength range within which actual industrial CCD cameras receive radiative energy. However, until now, few studies have been conducted on developing reconstruction formulas over the visible wavelength range. The chief aim of this paper is to develop an improved reconstruction model within the visible range. Nu-

*Project supported by the State Key Program of National Natural Science Foundation of China (Grant No 60534030) and Program for Changjiang Scholars and Innovative Research Team in University (Grant No IRT0434).

†Corresponding author. E-mail: wangfei@cmee.zju.edu.cn

merical simulation case is used to check the model. Results and discussions are also given.

2. Three-dimensional temperature distribution reconstruction model within visible range

2.1. Simulation system

A 3D simulation furnace with a size $0.4\,\mathrm{m} \times 0.4\,\mathrm{m} \times 0.4\,\mathrm{m}$ was divided into $7 \times 7 \times 7$ volume elements, as shown in Fig.1, in which the origin of the coordinate system is at the centre of the system. The CCD target plane was divided into 30×30 elements. Eight CCD cameras were chosen to obtain radiative energy images, four of which were mounted on the left and right walls, two per each side. Another four cameras were mounted on the front and back walls, also two per each side (only the cameras on the left and right walls are marked out in Fig.1). The simulation system is full of CO_2, N_2 and carbon particles, which are assumed to be an absorbing, emitting, and anisotropically scattering medium. The carbon particles were specified to be of uniform diameter 30μm, and the volume fraction of CO_2 was assumed to be 0.21.

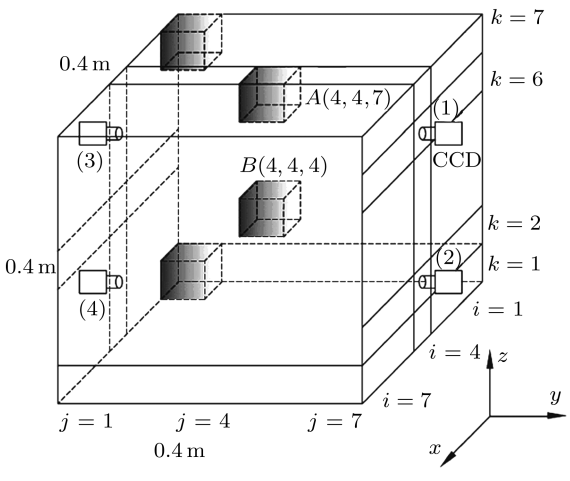


Fig.1. Simulation furnace.

The radiative properties of carbon particles were calculated using Mie theory.[13] It was thought in Ref.[14] that the complex index of refraction of carbon particle is 1.93 (1-0.53i) at wavelength of $2\,\mu$m, which is the average wavelength of radiation in pulverized-coal combustion, and this value can be used throughout the combustion process. In Fig.2 the results are shown with x being the size parameter.

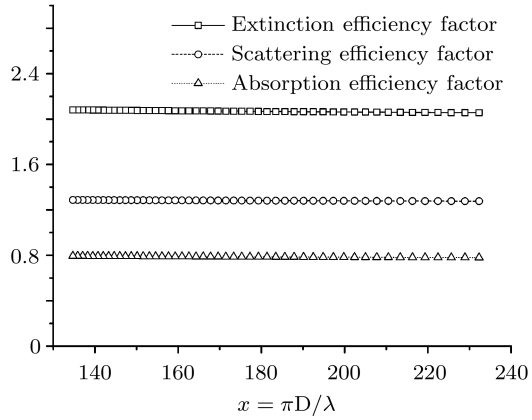


Fig.2. Radiative properties of carbon particles.

From Fig.2 radiative parameters of carbon particles almost do not vary with the wavelength in the visible range. For particle concentration of 2×10^8 per cubic metre, the extinction coefficient and scattering coefficient were calculated to be $0.29\,\mathrm{m}^{-1}$ and $0.18\,\mathrm{m}^{-1}$.

2.2. Reconstruction model within visible range

In Fig.1 the 3D simulation furnace is assumed to be divided into N volume elements. In the actual furnace, the temperature on the walls is much lower than that in the furnace, so the radiative energy emitted by the walls can be ignored. There are N unknown temperature values to solve. CCD target plane is assumed to be divided into M pixels so that M equations can be obtained as follows:

$$\begin{aligned} f_1(T_1, T_2, \ldots, T_N) &= P_1, \\ f_2(T_1, T_2, \ldots, T_N) &= P_2, \\ &\vdots \\ f_M(T_1, T_2, \ldots, T_N) &= P_M, \end{aligned} \tag{1}$$

where P_j is the radiative energy received by each pixel on the CCD target plane, f_j represents the radiative energy propagation and imaging process, T_i is temperature of each volume element i; j=1, 2, ..., M. $i = 1, 2, \ldots, N$.

The Monte Carlo method[11] was employed to study radiative energy propagation and the imaging model[15] was used to calculate the imaging process.

Within the response wavelength range of CCD camera, the energy emitted by volume element i in pulverized coal flame was calculated using

$$E_i = 4\alpha\sigma_0\Delta V_i \cdot T_i^4, \tag{2}$$

where α is the Planck mean absorption coefficient, in unit of m^{-1}, σ_0 is the Stefan–Boltzmann constant, ΔV_i is the volume of a volume element.

The radiative energy emitted by the volume element i arriving at the pixel j on the CCD target plane is expressed as

$$E_{i\to j} = E_i\alpha_{i\to j}, \tag{3}$$

where $\alpha_{i\to j}$ is the energy fraction obtained from volume element i arriving at pixel j on the CCD target plane.

Within the visible wavelength range, the Planck mean absorption coefficient is calculated using the following equation:

$$\alpha = \frac{\int_{\lambda_1}^{\lambda_2}(\alpha_\mathrm{g}+\alpha_\mathrm{p})\,e_{b\lambda}\mathrm{d}\lambda}{\sigma_0 T_i^4}, \tag{4}$$

where α_g and α_p are gas absorption coefficient and particle absorption coefficient respectively and λ_1, λ_2 are low and high CCD response wavelength respectively.

From Eqs.(2), (3) and (4) the following equation can be obtained

$$\begin{aligned} E_{i\to j} &= E_i\alpha_{i\to j} \\ &= 4\Delta V_i\alpha_{i\to j}\int_{\lambda_1}^{\lambda_2}(\alpha_\mathrm{g}+\alpha_\mathrm{p})\,e_{b\lambda}\mathrm{d}\lambda. \end{aligned} \tag{5}$$

The response wavelength range of the CCD camera is 0.4–0.7 μm which is the wavelength range of visible light. Spectral absorption coefficients of CO_2 are considered to be zero in this wavelength range. Equation (5) can be simplified and the following equation can be gained:

$$\begin{aligned} E_{i\to j} &= 4\Delta V_i\alpha_\mathrm{p}\alpha_{i\to j}\int_{\lambda_1}^{\lambda_2} e_{b\lambda}\mathrm{d}\lambda \\ &= A_{i\to j}T_{Ei}, \end{aligned} \tag{6}$$

where

$$A_{i\to j} = 4\Delta V_i\alpha_\mathrm{p}\alpha_{i\to j}, \tag{7}$$

and

$$T_{Ei} = \int_{\lambda_1}^{\lambda_2} e_{b\lambda}\mathrm{d}\lambda. \tag{8}$$

Then the reconstruction model can be deduced according to Eqs.(1) and (6):

$$\begin{aligned} \sum_{i=1}^{N}(A_{i\to 1}T_{Ei}) &= P_1, \\ \sum_{i=1}^{N}(A_{i\to 2}T_{Ei}) &= P_2, \\ &\vdots \\ \sum_{i=1}^{N}(A_{i\to M}T_{Ei}) &= P_M. \end{aligned} \tag{9}$$

We rewrite Eq.(9) in the matrix form

$$\boldsymbol{A}\boldsymbol{T_E} = \boldsymbol{E},\ \boldsymbol{A}\in\boldsymbol{R^{M\times N}},\ \boldsymbol{T_E}\in\boldsymbol{R^N}, \boldsymbol{E}\in\boldsymbol{R^M}, \tag{10}$$

where $\boldsymbol{A}$ is the coefficient matrix and can be obtained using Monte Carlo method and imaging model. $\boldsymbol{E}$ is the energy vector and can be obtained by radiative energy images captured by CCD cameras. $\boldsymbol{T_E}$ is defined in Eq.(8).

Now it should be guaranteed that the coefficient matrix $\boldsymbol{A}$ will not have relationship with the unknown temperature.

Typical volume elements A and B in Fig.1 are used to investigate the relationships between $\alpha_{i\to j}$ and temperature, and typical results are illustrated in Fig.3. The pixel is chosen to be (15, 15) on the CCD target plane.

From Fig.3 it is found that $\alpha_{i\to j}$ does not vary with temperature. So according to Eq.(7) the coefficient matrix $\boldsymbol{A}$ is independent of temperature over the visible range. Thus the reconstruction steps can be described as follows:

a) Assume a temperature distribution;

b) Calculate coefficient matrix $\boldsymbol{A}$ in Eq.(10) according to Eq.(7) under the assumed temperature distribution;

c) Solve Eq.(10) for $\boldsymbol{T_E}$ according to radiative energy images;

d) Solve Eq.(8) for unknown temperature distribution.

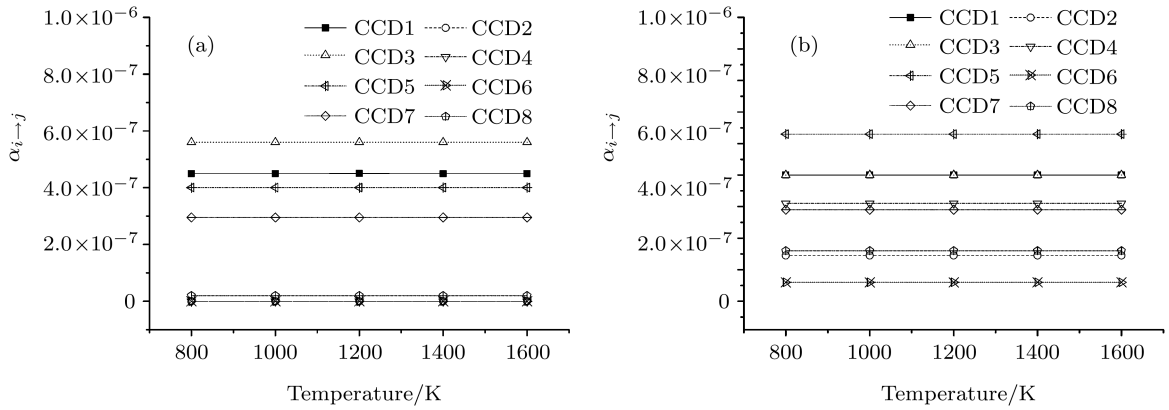


Fig.3. Variations of $\alpha_{i\to j}$ with temperature in typical volume elements. (a) Volume element A; (b) Volume element B.

3. Results and discussion

The assumed temperature distribution in the simulation system in Fig.1 is defined by the following equation

$$T(x,y,z)=950\left[\left(1-2\frac{|x-0.4/7|}{W}\right)\left(1-2\frac{|y+0.4/7|}{L}\right)\left(1-2\frac{|z|}{H}\right)+1\right]. \tag{11}$$

The temperature distribution in Ref.[11] has been modified and Eq.(11) is obtained. This assumed temperature distribution has a zigzag eccentric temperature distribution which is used to verify the validity of the algorithm developed in this paper, and the assumed temperature distribution on the typical cross section $k=4$ in Fig.1 is illustrated in Fig.4.

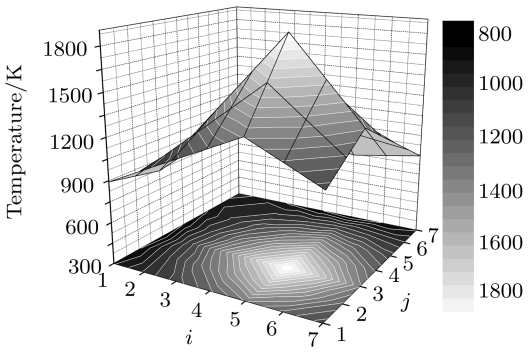


Fig.4. Assumed temperature distribution on the typical cross section $k=4$.

Least square QR-factorization (LSQR) was introduced to solve the reconstruction Eq.(10) and details about LSQR can be found in Refs.[16,17].

In order to simulate measurement errors, random errors of normal distribution with zero average value and mean square deviation σ are added to the energy $\boldsymbol{E}$ in Eq.(10)

$$\boldsymbol{E}_{\rm err}=(\mu+\sigma\xi)\boldsymbol{E}+\boldsymbol{E}, \tag{12}$$

where average value μ=0, ξ is a random variable of standard normal distribution, $-2.576<\xi<2.576$.

Here σ is assumed to be 0.01. Iteration times are 50 and residual norms are shown in Fig.5.

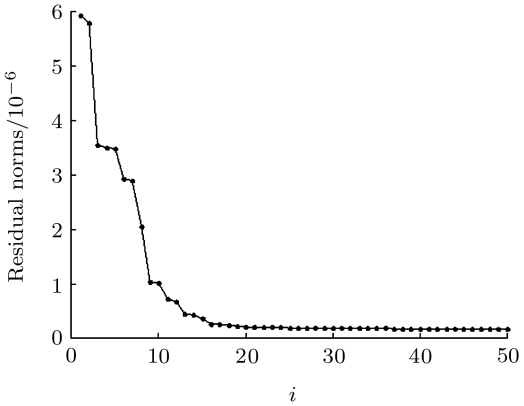


Fig.5. Residual norms.

Some values of $\boldsymbol{T_E}$ obtained may be negative which are meaningless. So the modified method is

used in order to avoid those negative values of $\boldsymbol{T_E}$:

$$\begin{aligned} T'_{Ei} &= T_{Ei}, && T_{Ei} > T_{E\min};\\ T'_{Ei} &= T_{Ei} + T_{E\min}, && 0 < T_{Ei} \le T_{E\min};\\ T'_{Ei} &= T_{E\min}, && T_{Ei} \le 0;\\ T_{E\min} &= 7.60e-4, \end{aligned} \tag{13}$$

where T_{Ei} is the value for original $\boldsymbol{T_E}$, and T'_{Ei} is the modified value.

Standard $\boldsymbol{T_E}$ in Eq.(8) at different temperatures can be calculated, the results are shown in Fig.6.

After $\boldsymbol{T_E}$ was obtained by solving Eq.(10), the reconstructed temperature distribution can be obtained through Fig.6. Reconstructed results of $\boldsymbol{T_E}$ on the cross section $k = 3$ and $k = 4$ are shown in Fig.7.

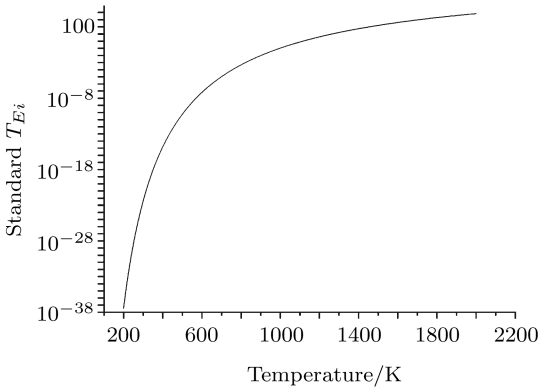


Fig.6. Standard T_E distribution.

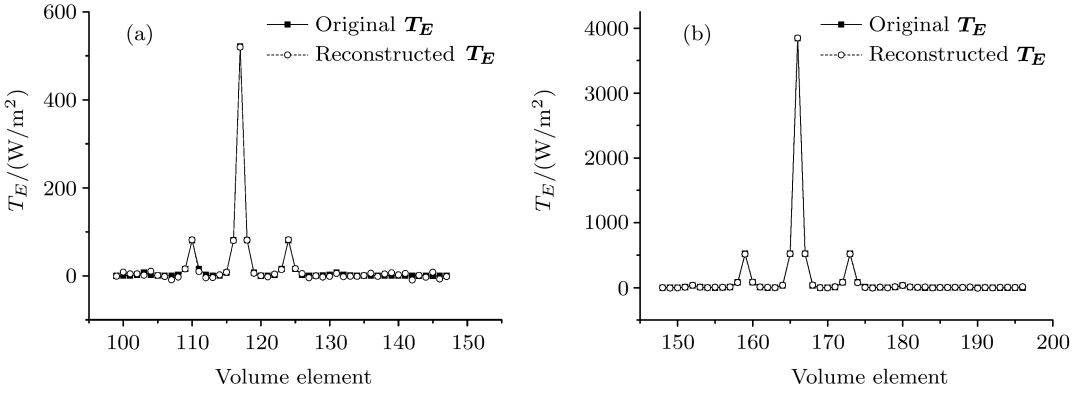


Fig.7. Reconstructed $\boldsymbol{T_E}$ on cross sections $k = 3, 4$. (a) Cross section $k = 3$; (b) cross section $k = 4$.

The serial number of the abscissa is as the following sequence: $(1,1,1) \to (2,1,1) \to \cdots \to (7,1,1) \to (1,2,1) \to (2,2,1) \to \cdots \to (7,7,1) \to (1,1,2) \to \cdots \to (7,7,7)$ as shown in Fig.1.

The reconstructed temperature distributions on the cross sections $k = 3, 4$ are shown in Fig.8.

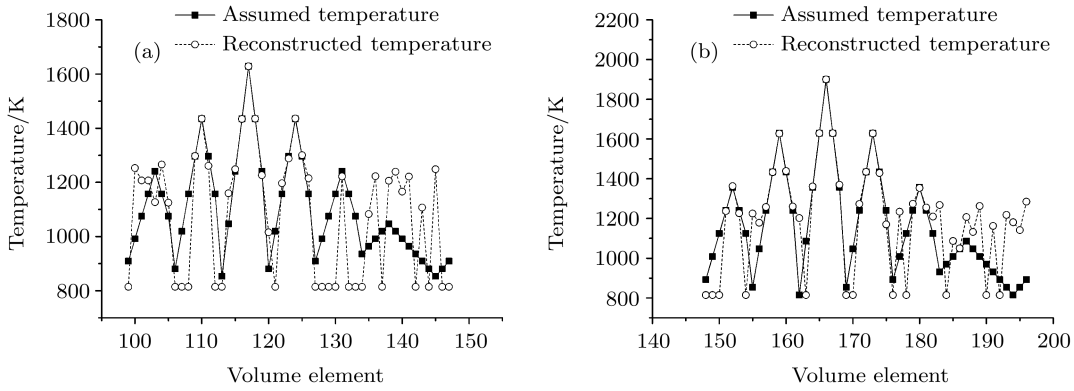


Fig.8. Reconstructed temperature distribution on cross sections $k = 3, 4$. (a) Cross section $k = 3$; (b) cross section $k = 4$.

In a large-scale furnace high-temperature areas are more concerned by scientists so we give Fig.9 to show the temperature distribution on cross section $k = 4$.

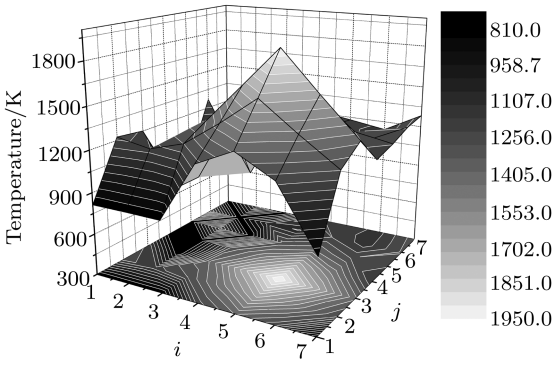


Fig.9. Reconstructed temperature distribution on cross section $k = 4$.

It is found that the reconstructed results in low-temperature areas have some fluctuations and high-temperature areas can be well reconstructed. It is also worth noting that the position of the highest temperature can be reconstructed exactly. Reconstructed temperature distribution can reproduce the features of the assumed temperature distribution.

The average relative error for the whole temperature distribution reconstruction and relative error for the highest-temperature reconstruction have also been calculated. They are 14.7% and 0.0090% respectively. The total relative error is mainly due to errors in low-temperature areas. The relative error for highest-temperature reconstruction is very small.

The reasons why the reconstructed results in the low-temperature areas had fluctuations may be that, as the temperature increases, the value of $\boldsymbol{T_E}$ increases much more quickly as shown in Fig.6, i.e. if the differences between temperatures are large, the gap between the corresponding values of $\boldsymbol{T_E}$ will be very huge. This will bring difficulties for solving the reconstruction equation (10). Moreover, Eq.(10) itself is an ill-posed equation, which will bring instability for solving Eq.(10), too. The assumed zigzag eccentric temperature distribution may be also hard to be reconstructed well. Better reconstructed results may be expected if smooth temperature distribution is to be reconstructed.

4. Conclusions

A reconstructed model of 3D temperature distribution within the visible wavelength range has been developed in this paper. Numerical simulation was used and its results showed that the temperature distribution corresponding to high-temperature areas can be well reconstructed but results in low-temperature areas have some fluctuations. The position of the highest temperature can be reconstructed exactly, and the total relative error is mainly due to errors in low-temperature areas. The relative error for highest temperature is quite small. Better results may be expected if the temperature distribution to be reconstructed is smooth.

References

[1] Li H Y and Ozisik M N 1992 *Journal of Heat Transfer* **114** 1060
[2] Li H Y 1994 *JQSRT* **52** 755
[3] Li H Y 1997 *Num. Heat Transfer* Part B **31** 251
[4] Liu L H, Tan H P and Yu Q Z 2001 *Int. J. Heat Mass Transfer* **44** 63
[5] Liu L H and Tan H P 2001 *JQSRT* **68** 559
[6] Silvaneto A J and Ozisik M N 1995 *JQSRT* **53** 397
[7] Huang Q X, Liu D, Wang F, Yan J H, Chi Y and Cen K F 2007 *Acta Phys. Sin.* **56** 6742 (in Chinese)
[8] Zhou H C, Han S D, Sheng F and Zheng C G 2002 *JQSRT* **72** 361
[9] Lou C and Zhou H C 2005 *Combustion and Flame* **143** 97
[10] Guan Z Q, Abe Y, Jiang D H, Lin H, Yamazaki Y and Wu C X 2004 *Chin. Phys.* **13** 105
[11] Farmer J T and Howell J R 1994 *J. Thermophys. Heat Trans.* **8** 133
[12] Wang Z J, Dong L F and Shang Y 2005 *Acta Phys. Sin.* **54** 880 (in Chinese)
[13] Modest M F 1993 *Radiative Heat Transfer* (New York: McGraw-Hill) p383
[14] Smoot L D and Pratt D T 1979 *Pulverized-Coal Combustion and Gasification* (New York: Plenum) p92
[15] Wang F, Liu D, Huang Q X, Yan J H and Cen K F 2006 *The 5th International Symposium on Measurement Techniques for Multiphase Flows* (Macao) p629
[16] Paige C C and Saunders M A 1982 *AMC Transactions Math.* **8** 43
[17] Paige C C and Saunders M A 1982 *AMC Transactions Math.* **8** 195